Polymer 156 (2018) 10–21

Contents lists available at ScienceDirect

Polymer

journal homepage: www.elsevier.com/locate/polymer

A pyrene-functionalized polytyrosine exhibiting aggregation-induced emission and capable of dispersing carbon nanotubes and hydrogen bonding with P4VP

Ahmed F.M. EL-Mahdy[a,b], Shiao-Wei Kuo[a,c,*]

[a] Department of Materials and Optoelectronic Science, National Sun Yat-Sen University, Kaohsiung, 80424, Taiwan
[b] Chemistry Department, Faculty of Science, Assiut University, Assiut, 71516, Egypt
[c] Department of Medicinal and Applied Chemistry, Kaohsiung Medical University, Kaohsiung, Taiwan

HIGHLIGHTS

- Pyrene-functionalized polytyrosine has been synthesized via a ring-opening polymerization of 1,6-diaminopyrene as an initiator.
- Pyrene-$2NH_2$ is an ACQ material, whereas it transformed into an AIE material after incorporation into the backbone of the polytyrosine.
- Pyrene-PTyr blending with poly(4-vinylpyridine) (P4VP) to form supramolecular pyrene-PTyr/P4VP systems.
- Utilization of pyrene-PTyr polypeptide as an effective dispersant for multi-walled carbon nanotubes.

ARTICLE INFO

Keywords:
Polypeptides
Hydrogen bonding
Carbon nanotube
AIE

ABSTRACT

A new pyrene-functionalized polytyrosine (pyrene-PTyr) by using L-tyrosine-*N*-carboxyanhydride as monomer synthesized through simple ring-opening polymerization with 1,6-diaminopyrene (pyrene-$2NH_2$) as the initiator. UV–Vis absorption spectra revealed that the absorption maxima of pyrene-$2NH_2$ and pyrene-PTyr were correlated to the solvent polarity. The photophysical properties of pyrene-$2NH_2$ and pyrene-PTyr were investigated using photoluminescence (PL) spectroscopy, which revealed that pyrene-$2NH_2$ displayed aggregation-caused quenching behavior, which transformed to aggregation-induced emission after incorporation into the rigid rod chains of polytyrosine. In addition, pyrene-PTyr could be blended with poly(4-vinylpyridine) (P4VP) to form supramolecular pyrene-PTyr/P4VP systems stabilized through hydrogen bonding. Thermal analyses revealed, through the appearance of the single T_g behavior, that all of the pyrene-PTyr/P4VP blends were completely miscible. FTIR spectral analyses revealed strong hydrogen bonding between in pyrene-PTyr/P4VP blends. Moreover, X-ray diffraction analyses indicated that the secondary structure for pyrene-PTyr converted from the β-sheet to the random coil conformation after intermolecularly hydrogen bonding with P4VP. Furthermore, photographs, PL spectra, and transmission electron microscopy images indicated that the pyrene-PTyr polypeptide was an effective dispersant for multi-walled carbon nanotubes (MWCNTs), stabilized through strong π-stacking between the pyrene units of pyrene-PTyr and the surfaces of the MWCNTs.

1. Introduction

Polypeptides have received much attention in the last decade because of their close structural relationship with proteins and their many applications in various fields, including gene and drug delivery as well as tissue engineering [1–3]. Polypeptides can form three kinds of hierarchical secondary structures in solution and in aggregation states: α-helices, which can exist as rigid rod–like polymers stabilized by using intramolecular (or intra-chain) hydrogen bonding, β-sheets stabilized through intermolecular hydrogen bonding; and random coils [4,5]. The degree of polymerization exerts a high degree of control over the secondary structure of a polypeptide; for example, the secondary structures of polypeptides will be α-helices when the degree of polymerization is greater than 18 [6]. Several new synthetic polypeptides have been syntheses by using *N*-carboxyanhydrides and amino-functionalized monomers by ring-opening polymerization (ROP) [7,8]. Furthermore, many examples have appeared of the incorporation of poly(ethylene oxide) [9,10], poly(ethyl oxazoline) [11], poly(ε-

* Corresponding author. Department of Materials and Optoelectronic Science, National Sun Yat-Sen University, Kaohsiung, 80424, Taiwan
E-mail address: kuosw@faculty.nsysu.edu.tw (S.-W. Kuo).

https://doi.org/10.1016/j.polymer.2018.09.052
Received 30 July 2018; Received in revised form 17 September 2018; Accepted 25 September 2018
Available online 26 September 2018
0032-3861/

caprolactone) [12], and polyhedral oligomeric silsesquioxane (POSS) [13,14] into the main or side chains of polypeptides, producing poly (peptide-*b*-nonpeptide) copolymers that have attractive applications for drug delivery and molecular recognition. On the other hand, the formation of miscible polymer blends stabilized through noncovalent interactions (e.g., hydrogen bonding [15,16], dipole–dipole [17,18], or π–π interaction [19]) has become a convenient and influential method for elaborating functional polypeptides. Among these noncovalent interactions, hydrogen bonding is a particularly powerful tool, due to its versatility and strength, when preparing multicomponent assemblies [20,21]. Hydrogen-bonded assemblies could possess fascinating properties, but only a few reports describe the applications of multicomponent supramolecular assemblies. For example, we have previously described the blending of poly(γ-ethyl-L-glutamate) (PELG), poly(γ-methyl-L-glutamate) (PMLG), and poly(γ-benzyl-L-glutamate) (PBLG) and with random-coil nonpeptide polymers, including phenolic resin and polyvinylphenol (PVPh), in which intermolecular hydrogen bonding occurs between the carbonyl units of polypeptides and the hydroxyl units of phenolic or PVPh [22,23]. Furthermore, we have demonstrated that intermolecular hydrogen bonding exists between polytyrosine (PTyr) and poly(4-vinylpyridine) (P4VP) in MeOH and DMF solutions [24]. The secondary structures formed in these blending systems are strongly affected by the strengths of the hydrogen bonding interactions in the various common solvents.

Luminescent (fluorescent or phosphorescent) material, which emits light from its excited electronic state after the visible or UV light absorption, have received great attention for their applications (e.g., as luminescent sensors) in many disciplines, including materials science, chemistry, and biology [25–27]. For example, pyrene, one of the most widely used fluorescent compounds, has been applied as a luminescent probe in many applications [28–30]. In most research studies, the fluorescence of organic compounds is generally studied in dilute solution, such that no intermolecular interactions occur between the organic fluorescent molecules [31–33]. Nevertheless, many organic fluorophores that possess delocalized π-conjugated systems (e.g., pyrene, carbazolyl, and dansyl systems) emit strongly from their dilute solutions, but very weakly from their concentrated solutions or when aggregated (e.g., in the solid state) [34]. Such behavior arises mainly from strong π-stacking, which leads to excimer formation; this phenomenon is known as aggregation-caused quenching (ACQ). Moreover, the ACQ phenomenon might not be desirable in some optoelectronic usages [e.g., organic light-emitting diodes (OLEDs)] in which the fluorescent materials in the solid state might experience severe ACQ effects [35]. To solve this problem, many fluorescent organic materials have been synthesized to emit efficiently in solid state as well as in solution state. The opposite phenomenon of ACQ has been reported recently: Tang *et al.* discovered that 1-methyl-1,2,3,4-pentaphenylsilole exhibits weak fluorescence in dilute solution; however, stronger fluorescence in concentrated solution or in aggregation state [36–38]; this phenomenon was called “aggregation-induced emission” (AIE) behavior. The AIE mechanism has been explained as follows: in a dilute solution, the five phenyl rings undergo the dynamic intramolecular rotations (IRs) where strongly quench the excited state and lead to the absence of emission of the luminophore. In addition, the silole molecules could not bundle through the face-to-face π–π intermolecular interaction. The combination of IRs and π–π interactions in solution have a strong effect of turning off the luminescence of the excited state. Consequently, AIE materials have become highly interesting fluorescent materials with many applications (e.g. as luminescence probes, OLEDs, and bio-imaging agents). Furthermore, Hong *et al.* reported the AIE behavior of tetraphenyl thiophene, discovering that its incorporation into a synthetic polypeptide (PBLG) decreased the AIE effect strongly as a result of the steric effects of the α-helices of the polypeptide [39]. Nevertheless, very few papers describe the ACQ and AIE effects of luminescent molecules after their incorporation into polypeptides.

Because of their unique one-dimensional structures and strongly π-conjugated systems, carbon nanotubes (CNTs) possess many attractive thermal, mechanical, and optoelectronic properties [40]. The high strength of the π–π intermolecular interactions of CNTs with photoluminescent aromatic materials (e.g., pyrene derivatives) can result in strong quenching of the latter's emission [41,42]. Consequently, pyrene/CNT systems have been applied widely as biosensors for the determination of proteins, DNA, and RNA [43,44]. Nevertheless, the polarized surfaces of CNTs, arising from intertubular van-der Waals force, facilitate the highly hydrophobic formation and the insoluble aggregate [45], thereby prohibiting their assembly with other useful structures. Several diverse approaches have been developed to improve the dispersion of CNTs, including modification of their surfaces through the covalent and noncovalent attachment of solubilizing groups. In an example of covalent modification, the graft-form approach has been used to functionalize CNT surfaces with amino groups, which readily to react with *N*-carboxyanhydrides to produce covalent polypeptide/CNT composites [46,47]. Although this approach can improve the dispersion of the CNTs, it changes their intrinsic properties and, thereby, makes them less suitable for many applications [48]. In contrast, the noncovalent approach can improve the dispersion of CNTs while preserving their intrinsic properties. Many agents (e.g., conjugated polymers, biomaterials, surfactants) have been used to improve the dispersibility of CNTs [49]. Among the tested biomaterials, polypeptides display high efficiency when used as dispersive agents. The α-helical conformation of polypeptides limits the surface energy of CNTs, thereby improving their dispersion [50,51]. The development of new noncovalent CNT/polypeptide composites would appear to enhance their biophysical and biomedical applications.

In our previous studies, the diamino-methoxytriphenylamine (TPA-NH_2) or bisaminophenyl phenylpyridine (pyridine-NH_2) were used as initiators for the synthesis of triphenylamine-functionalized polytyrosine (PTyr-TPA) and pyridine-functionalized polytyrosine (pyridine-PTyr) [52,53]. TPA-NH_2 and pyridine-NH_2 exhibited ACQ phenomena which converted to AIE materials after incorporation the polytyrosine and produced AIE-polytyrosines. On the other hand, Hong *et al.* also reported the synthesis of a pyrene-functionalized and a non-AIE poly(γ-propargyl-l-glutamate) polypeptide by the ring opening polymerization of pyren-1-ylmethanamine (Py-NH_2) which its amino group not directly attached to the pyrenyl ring [54]. Based on our knowledge, the preparation of PTyr combines the AIE behavior and the pyrene moiety which capable to disperse of CNTs, have never previously reported. In addition, the utilization of 1,6-diaminopyrene (pyrene-$2NH_2$) which its amino groups directly attached to the pyrenyl ring as initiator have also never previously reported. In this study, we employed pyrene-$2NH_2$ as a diamine-functionalized initiator for the synthesis of the polypeptide pyrene-PTyr through living ring-opening polymerization of Tyr-NCA at room temperature (Scheme 1). We recorded ultraviolet–visible (UV–Vis) absorption and photoluminescence (PL) spectra to examine the photo-physical characteristics of pyrene-$2NH_2$ and pyrene-PTyr. This new polypeptide, pyrene-PTyr, possesses phenolic hydroxyl groups that can hydrogen bonded with the pyridyl groups of poly(4-vinylpyridine) (P4VP). The hydrogen bonding, miscibility, and secondary structural conformations of various pyrene-Tyr/P4VP blends were also investigated. In addition, we have studied the dispersibility of multiwalled carbon nanotubes (MWCNTs) with pyrene-PTyr.

2. Experimental section

2.1. Materials

Pyrene was used as received from Acros. 10 wt% Pd/C, hydrazine hydrate (98%), and triphosgene were purchased from Alfa Aesar. L-Tyrosine compound was obtained from the MP Biomedicals. Glacial acetic acid was acquired from Fluka. P4VP (160,000 g/mol) was purchased from Aldrich. Ethanol, dimethylformamide (DMF), THF,

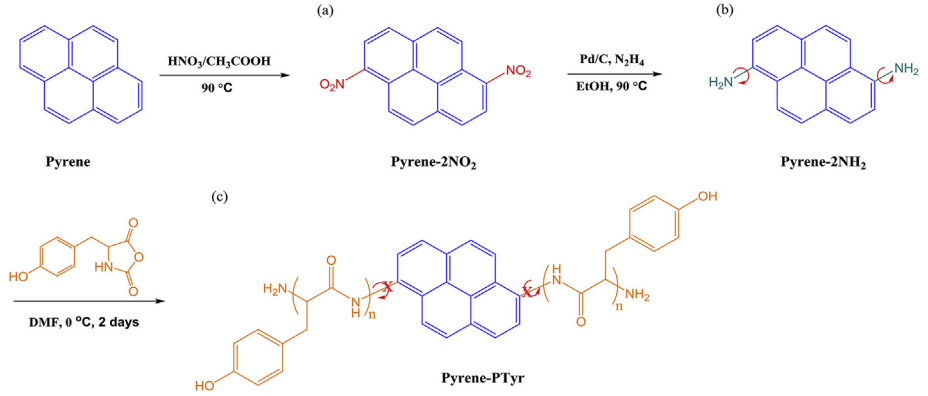

Scheme 1. Schematic representation of the synthesis of (a) pyrene-2NO_2, (b) pyrene-2NH_2 and (c) pyrene-PTyr.

acetonitrile, methanol, dichloromethane (DCM), dimethylsulfoxide (DMSO), and acetone were obtained from Merck; they were all distilled over calcium hydride prior to use. MWCNTs was obtained from the Centron Biochemistry Technology. L-Tyrosine *N*-carboxyanhydride (Tyr-NCA) monomer was prepared previously [24].

2.2. Characterization

FTIR spectrum of the synthesized samples was recorded using the Bruker Tensor 27 FTIR spectrometer; 64 scans were gathered at a spectral resolution of 1 cm^{-1}. Nuclear magnetic resonance (NMR) spectrum of the prepared samples was recorded using the Agilent VMRS-600 NMR spectrometer. The samples were dissolved in deuterated solvents (DMSO-d_6, $CDCl_3$); tetramethylsilane (TMS) was used as the external standard. The molecular weight of the polypeptide pyrene-PTyr was measured through the gel permeation chromatography (GPC) with three ultrastragel columns (500, 580, and 10 Å) and a 410 differential 45 refractometer connected in series and the DMF solvent was used as the diluent. The molecular weight of the polypeptide pyrene-PTyr was also measured through mass-analyzed laser desorption/ionization (MALDI-TOF) mass spectrometry, using a Bruker Daltonics Autoflex III spectrometer. DSC analysis was performed by the Q-20 apparatus (TA) under a N_2 atmosphere. The synthesized samples (3 mg) in a fixed and sealed aluminum pan were heated from 40 to 200 °C (heating rate: 20 °C/min). Thermogravimetric analysis (TGA) was measured using a TA Q-50 thermogravimetric instrument. The synthesized samples were heated from 40 to 800 °C (heating rate: 20 °C/min) and under the N_2 atmosphere. X-ray patterns of blend samples were performed by using the BL17A1wiggler beam line. A single crystal of triangular bent Si (111) was employed to produce the monochromatic beam featuring the wavelength of 1.33 Å. Samples for UV–Vis and PL spectroscopy were dissolved in suitable organic solvents and placed in a small quartz cell (0.2 × 1.0 × 4.5 cm^3). The UV–Vis absorption spectrum was determined using optics DT 1000 and CE 376 spectrophotometers. The PL spectra emission spectrum was recorded using a LabGuide X350 spectrometer. TEM images of the prepared samples were measured by the JEOL-2100 transmission electron microscope.

2.3. 1,6-Dinitropyrene (Pyrene-2NO_2)

A solution of pyrene (5.00 g, 24.8 mmol) in glacial acetic acid (50 mL) was stirred at 90 °C. A mixture of nitric acid (70%, 3.8 mL) and glacial acetic acid (10 mL) was added quickly, and then the mixtures were stirred for 1 h at the 90 °C. The yellow suspension was cooled; the precipitate was collected by filtration and washed with CH_3OH. The product was a mixture including the 1,6-dinitropyrene, 1,3-dinitropyrene, and 1,8-dinitropyrene; this mixture was used in the next step without purification.

2.4. 1,6-Diaminopyrene (Pyrene-2NH_2)

The dinitropyrene mixture (6.0 g) and 10% Pd/C (0.40 g) were suspended in ethanol (160 mL). The suspension was heated at 90 °C for 10 min under the N_2 atmosphere and then hydrazine monohydrate (8.0 mL) was added slowly. The resulting suspension was stirred at 90 °C for 48 h. The mixture was filtered hot and then the filtrate was cooled to room temperature, giving a mixture of 1,6-diaminopyrene, 1,3-diaminopyrene and 1,8-diaminopyrene. Silica gel column chromatography (eluent: 10% ethyl acetate/DCM) was used to separate the diaminopyrenes (1,6-diaminopyrene: R_f = 0.8; 1,3-diaminopyrene: R_f = 0.4; 1,8-diaminopyrene: R_f = 0.35). 1,6-Diaminopyrene (0.75 g, 20%). FTIR (KBr): 3424–3350 (2NH_2 stretching), 1622, 1598, 1499, 1433, 1324, 1282, 1137, 828, 709, 529 cm^{-1}. ^{1}H NMR (500 MHz, DMSO-d_6, Scheme S1): 7.77 (d, 4H, J = 10 Hz; H_b, H_d), 7.67 (d, 2H, J = 10 Hz; H_c), 7.25 (d, 2H, J = 10 Hz; H_a), 5.91 (broad, 4H; 2NH_2). ^{13}C NMR (125 MHz, DMSO-d_6): 142.28 (C_1), 126.28 (C_4), 124.97 (C_6), 123.84 (C_3), 122.56 (C_2), 116.78 (C_5), 116.12 (C_8), 112.90 (C_7).

2.5. Pyrene-PTyr

A solution of Tyr-NCA monomer (3.00 g, 14.5 mmol, 44 eq.) in dry DMF (20 mL) was cooled to 0 °C for 20 min and then a solution of pyrene-2NH_2 (76.4 mg, 0.330 mmol, 1 eq.) in DMF (5 mL) was added dropwise. The mixtures were stirred at 0 °C for 72 h and then the polypeptide was precipitated through the addition of diethyl ether (Et_2O). The precipitate were purified through dissolution into methanol and reprecipitation from Et_2O to yield a pale yellow powder (2.4 g), which was dried under vacuum at 40 °C overnight. Pyrene-PTyr: T_g = 154.2 °C; FTIR (KBr, cm^{-1}): 3282 (NH), 3020, 2922, 1651, 1626, 1515, 1440, 1236, 1109, 828, 538; ^{1}H NMR (500 MHz, DMSO-d_6): 2.88 (d, 2H, CH_2), 4.42 (t, 1H, CH), 6.71–6.57 (d, 2H, ArH), 6.99–6.82 (d, 2H, ArH), 7.93 (s, 1H, NH), 9.14 (s, 1H, OH). M_n = 5665 g mol^{-1}; PDI = 1.05 (GPC, Fig. S1).

2.6. Pyrene-PTyr/P4VP blends

The preparation of pyrene-PTyr/P4VP blends was dissolving various weight percentages in DMF solution. The blend solution was stirred at room temperature for 72 h and then the DMF was evaporated under reduced pressure at 70 °C for 72 h and then at 120 °C for 96 h to ensure its complete removal.

2.7. MWCNT dispersion in the presence of Pyrene-PTyr

A dispersion of MWCNTs (4 mg) in DMF (10 mL) was sonicated for 2 h. A solution of pyrene-PTyr (100 mg) in DMF (2 mL) was added dropwise and then the mixtures were sonicated for 2 h. After stirring at 25 °C for 48 h, the MWCNT dispersion was centrifuged (6000 rpm,

90 min) and then the supernatant was filtered through a PALL disc membrane filter (FP-450 PVDF filter). The obtained MWCNT/pyrene-PTyr composites were redispersed in desired solvents through sonication for 5 min.

3. Results and discussion

3.1. Synthesis of 1,6-diaminopyrene (Pyrene-2NH$_2$)

Scheme 1 presents the preparation of the diamine initiator monomer containing the pyrene unit, 1,6-diaminopyrene (pyrene-2NH$_2$). A mixture of dinitropyrenes (1,6-dinitropyrene, 1,3-dinitropyrene, and 1,8-dinitropyrene) was first synthesized through the nitration of pyrene in acetic acid in the presence of nitric acid. The mixture of dinitropyrenes was subjected to catalytic reduction mediated by hydrazine monohydrate in absolute ethanol and Pd/C. The desired monomer, 1,6-diaminopyrene, was isolated from the mixture of diaminopyrenes through silica gel column chromatography; it had a retention factor (R_f) of 0.8 when using 10% ethyl acetate in DCM as the eluent. The chemical structure of pyrene-2NH$_2$ was confirmed through FTIR and NMR spectroscopic analyses. The FTIR spectrum of pyrene-2NH$_2$ features three signals at 3424, 3384, and 3350 cm^{-1}, representing the two asymmetric and symmetric amino (2NH$_2$) groups [Fig. 1(a)]. The ^{1}H NMR spectrum of pyrene-2NH$_2$ features a broad signal at 5.91 ppm for the NH$_2$ groups, as well as aromatic protons in the range from 7.77 to 7.25 ppm [Fig. 2(a)]. The ^{13}C NMR spectrum of pyene-2NH$_2$ [Fig. S1(a)] features eight signals for the carbon nuclei of the pyrene unit, 142.28, 126.28, 124.97, 123.84, 122.56, 116.78, 116.12, and 112.90 ppm. Together, these data confirm the successful synthesis of 1,6-diaminopyrene (pyrene-2NH$_2$).

3.2. Synthesis of the Polypeptide Pyrene-PTyr

The polypeptide pyrene-PTyr was readily synthesized through ROP of Tyr-NCA monomer, initiated by the diamino-functionalized pyrene-2NH$_2$, at room temperature in DMF. Using our previously reported method [24], we synthesized the Tyr-NCA monomer through a facile cyclization reaction of L-tyrosine with triphosgene in acetonitrile. In FTIR analysis of Tyr-NCA monomer [Fig. 1(b)], we observe two absorption peaks at 1852 and 1768 cm^{-1} for the two typical anhydride (C=O) stretching vibrations, as well as OH and NH stretching vibrations at 3314 and 3180 cm^{-1}, respectively. After ROP of Tyr-NCA in the presence of pyrene-2NH$_2$, FTIR spectrum [Fig. 1(c)] no longer featured the two anhydride signals of the Tyr-NCA monomer, but new strong absorption peaks appeared at 1651, 1626, and 1515 cm^{-1}, due to the amide units of pyrene-PTyr polypeptide backbone. Fig. 2(b) displays the ^{1}H NMR analysis of Tyr-NCA monomer; it exhibits a characteristic singlet at 9.34 ppm for the NH unit, a singlet at 9.02 ppm for phenolic OH unit, two signals at 6.95 and 6.68 ppm due to the aromatic CH groups from benzyl ring, a triplet at 4.69 ppm for the CH$_2$ group, and a doublet at 2.89 ppm for alkyl CH group. The formation of pyrene-PTyr was confirmed from its ^{1}H NMR spectrum [Fig. 2(c)], which featured a similar characteristic signal at 9.14 ppm for the NH groups, as well as a singlet at 7.93 ppm due to the phenolic OH unit. The signals of the CH groups which directly attached to the amide groups (NHCO) appeared at 4.53 and 4.42 ppm for the α-helical and β-sheet secondary structures. Furthermore, CH$_2$ groups of α-helical and β-sheet structures appeared at 2.88 and 2.72 ppm, respectively and other signals for aromatic protons (pyrenyl and phenyl) showed at chemical shifts from 6.99 to 6.57 ppm and at 8.21 ppm. Fig. S1(b) displays ^{13}C NMR analysis of Tyr-NCA monomer; the characteristic peaks of two anhydride C=O carbon were appeared at 171.52 and 152.47 ppm, the peak of the phenolic C–OH carbon was appeared at 156.38 ppm, and the signals of aromatic carbon atoms of the phenyl ring appeared at 130.79, 124.84, and 115.29. In addition, the characteristic signals of amino acid α-carbon (CCONH) and the benzylic PhCH$_2$ carbon atom were present at 67.30 and 35.11 ppm, respectively. Fig. S1(c) presents ^{13}C NMR analysis of the polypeptide pyrene-PTyr; the peaks of the amide (NHCO) carbon were appeared at 174.04 and 166.95 ppm, representing their α-helical and β-sheet conformations, respectively. Furthermore, amino acid α-carbon atoms of the α-helical and β-sheet conformations were appeared at 57.57 and 56.07 ppm, respectively. The molecular weights of the synthesized pyrene-PTyr were determined using MALDI-TOF mass spectrometry: a number-average molecular weight (M_n) of 2514.27 g mol^{-1}, a weight-average molecular weight (M_w) of 2597.69 g mol^{-1}, and a polydispersity index (PDI) of 1.03 (Fig. 3). Moreover, the mass differences between pairs of adjacent peaks were m/z 164, equal to a Tyr repeat unit. All results from FTIR, NMR, and MALDI-TOF mass spectral data were confirmed the preparation of the polypeptide pyrene-PTyr. Table 1 summarizes the degrees of polymerization of the polypeptide determined using GPC (Fig. S2) and MALDI-TOF mass spectrometry.

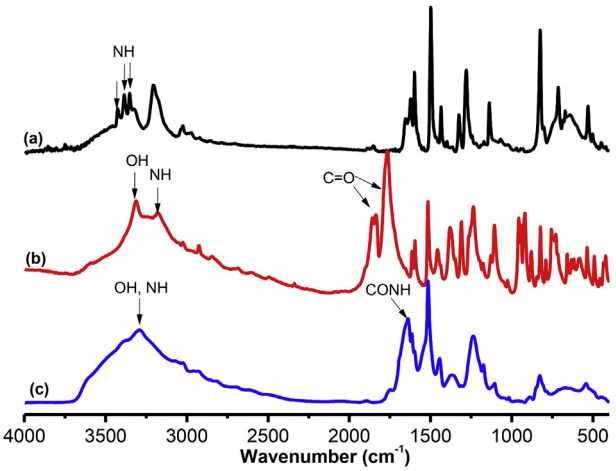

Fig. 1. Solid FTIR analyses of (a) pyrene-2NH$_2$, (b) Tyr-NCA, (c) pyrene-PTyr, recorded at room temperature.

3.3. Solubility, absorption, and photoluminescence

Pyrene-2NH$_2$ and pyrene-PTyr readily dissolved in highly polar solvent such as DMF, DMSO, and methanol. In addition, pyrene-2NH$_2$ exhibited good solubility in less-polar solvent such as DCM, THF, and acetone, whereas pyrene-PTyr was poorly soluble in these solvents. The excellent solubility of the polypeptide pyrene-PTyr in highly polar solvents suggested that it was a potential candidate for use in many optoelectronic applications. To understand the photo-physical behavior of pyrene-2NH$_2$ and the polypeptide pyrene-PTyr, we measured their UV–Vis absorption and fluorescence emission spectra in various polar solvents at room temperature. Fig. 4A presents the absorption spectra of pyrene-2NH$_2$ at a concentration of 10^{-4} M in various polar solvents; each absorption spectrum features two characteristic absorption bands: an absorption maximum band in the region 370–386 nm (representing the π–π* transition of the pyrenyl ring) and another in the region 419–435 nm (corresponding to the dimerization of a pair of pyrene units). Pyrene-2NH$_2$ exhibited the first of these absorption maxima at 370 nm in methanol, 374 nm in DCM, 378 nm in THF, 383 nm in DMF, and 386 nm in acetone. Thus, the absorption of pyrene-2NH$_2$ is strongly affected by the nature of the solvent. The strong red-shift of the absorption maximum of pyrene-2NH$_2$ in acetone arose because of host/guest intermolecular interaction between pyrene-2NH$_2$ and the environmental acetone, while blue-shift of the maximum in methanol arose from strong hydrogen bonding between the NH$_2$ units of pyrene-2NH$_2$ and methanol, leading to an increase in the stability of pyrene-2NH$_2$ in the ground state. Fig. 4B presents the absorption spectra of pyrene-PTyr at a 10^{-4} M concentration in DMF, DMSO, and methanol.

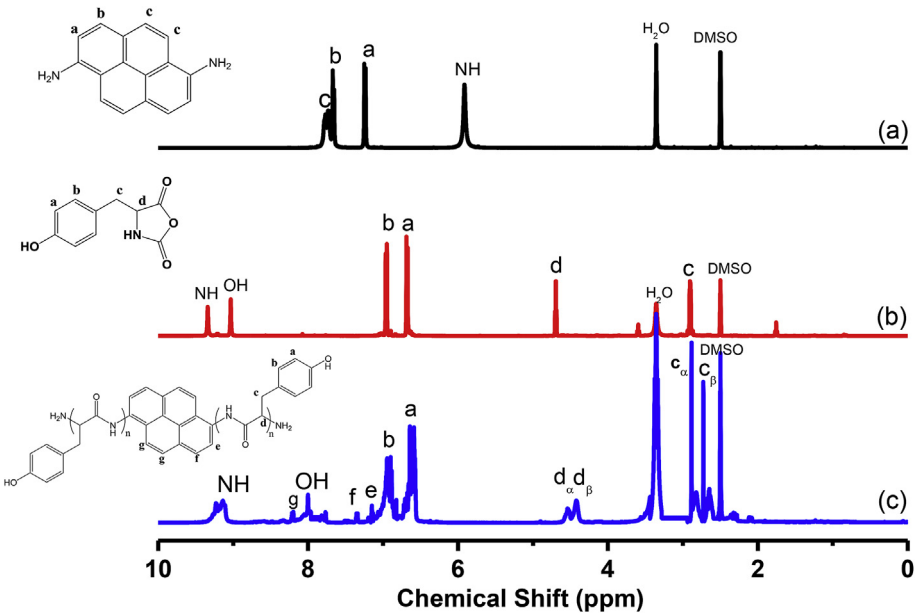

Fig. 2. ^{1}H NMR spectra of (a) pyrene-2NH$_2$, (b) Tyr-NCA, (c) pyrene-PTyr.

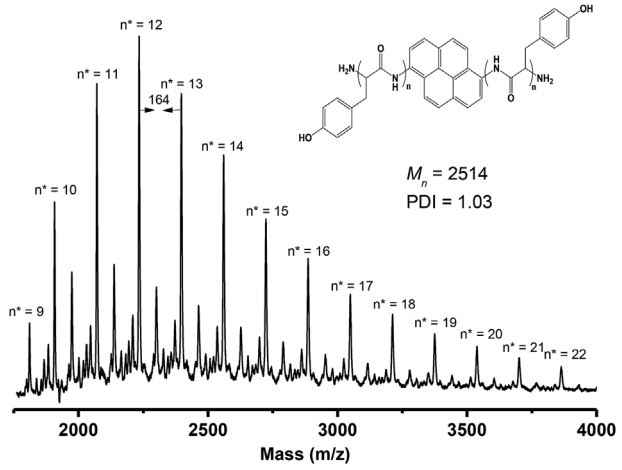

Fig. 3. MALDI-TOF mass analysis of pyrene-PTyr, *n** refers to the total number of incorporated tyrosine units in the two polytyrosine chains.

Table 1
Molecular weight and polydispersity index of the polypeptide pyrene-PTyr.

PDI[b]	M_n[b]	PDI[a]	M_n[a]	Polypeptide
1.05	5665	1.03	2514	pyrene-PTyr

[a] Determined from MADLI −TOF mass.
[b] Determined from GPC analysis.

The spectra featured absorption maxima at 385 and 368 nm, due to the π–π* transitions of the pyrenyl unit and of the phenyl unit in the tyrosine group, respectively. The absorption maximum was blue-shifted in methanol because of the strong hydrogen bonds between phenolic OH units in polypeptide and the solvent. These spectral data confirm that the absorption behavior of pyrene-2NH$_2$ and the polypeptide pyrene-PTyr were dependent on the solvent polarity.

Thomas *et al.* reported [52] that the fluorescence emission maximum of a pyrene-containing compound is strongly dependent on the polarity of the solvent; this phenomenon is known as the environment solvatochromism effect. We studied the solvatochromism effects of pyrene-2NH$_2$ and the polypeptide pyrene-PTyr by measuring their fluorescence emissions in solvents of various polarities. Fig. 5A presents the fluorescence emission spectra of pyrene-2NH$_2$ measured at a concentration of 10^{-4} M in solvents of various polarities. The emission maxima of pyrene-2NH$_2$ in DMF, methanol, acetone, THF, and DCM appeared at 470, 460, 458, 455, and 445 nm, respectively. Thus, the emission maximum increased upon increasing the solvent polarity. This solvatochromism and red-shifted emission in the polar solvents could be attributed to the strong hydrogen bonding interaction between amino (NH$_2$) groups of pyrene-2NH$_2$ and the carbonyl (C=O) or hydroxyl (OH) groups of polar DMF, acetone, and methanol solvent molecules, which increased the stability of the polar excited state of pyrene-2NH$_2$ resulting in a large change of the excited state dipole of the pyrene-2NH$_2$ and then accelerates the intramolecular charge-transfer process, this phenomenon is called as solvent relaxation [55,56]. In addition, this red shift can be imputed to the conversion of pyrene excimer from static excimer to dynamic excimer in the polar solvent. It has been reported that pyrene derivatives can be existed in dynamic or static excimers correlated to the generation way of a pyrene dimer. The dynamic static excimer was raised from the pyrene dimer generated in excited state, while the static excimer was raised from that dimer generated in ground state [57,58]. Thus, the strong hydrogen bond interaction between pyrene-2NH$_2$ and polar solvents isolated the pyrene-2NH$_2$ molecules to each other and thus induced the formation of the dimer in the excited state. We also investigated the fluorescence emissions of the polypeptide pyrene-PTyr at a 10^{-4} M concentration in DMF, DMSO, and methanol (Fig. 5B). In contrast to pyrene-2NH$_2$, pyrene-PTyr did not exhibit an environment solvatochromism effect. Pyrene-PTyr exhibited its fluorescence emission maxima at 457 nm in DMF, 458 nm in DMSO, and 453 nm in methanol. The fluorescence images in Fig. S3 reveal that pyrene-2NH$_2$ and pyrene-PTyr exhibited strong blue emissions in solution, suggesting that they are both promising blue-emitting materials.

To further investigation of fluorescence behaviors of these blue-emitting materials, the quantum yields (Φ_f) of pyrene-2NH$_2$ and pyrene-PTyr at a 10^{-4} M concentration in different solvents were performed using a concentration of 10^{-4} M of quinine sulfate in 1 N H_2SO_4 as a standard. As summarized in Table S1, the quantum yields of pyrene-2NH$_2$ were 47, 28, 32, 43, and 41 in DMF, methanol, acetone, THF, and DCM, respectively. On the other hand, the quantum yields of pyrene-PTyr in DMF, DMSO, and methanol were 24, 20, and 12, respectively. In addition, the quantum yield of pyrene-PTyr in the solid

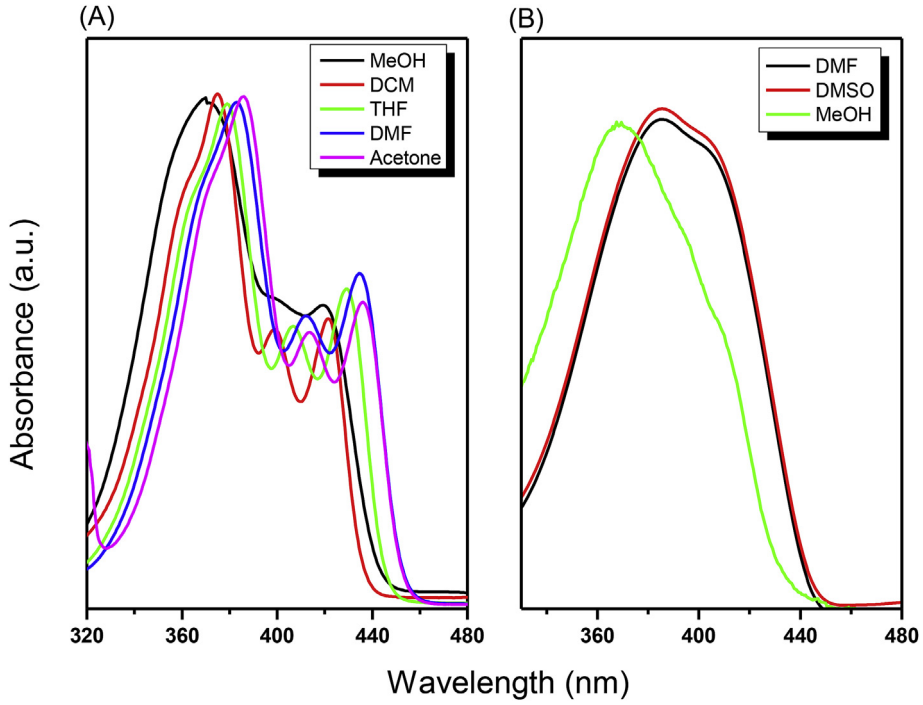

Fig. 4. Ultraviolet–visible absorption spectra of (A) pyrene-2NH_2 and (B) pyrene-PTyr.

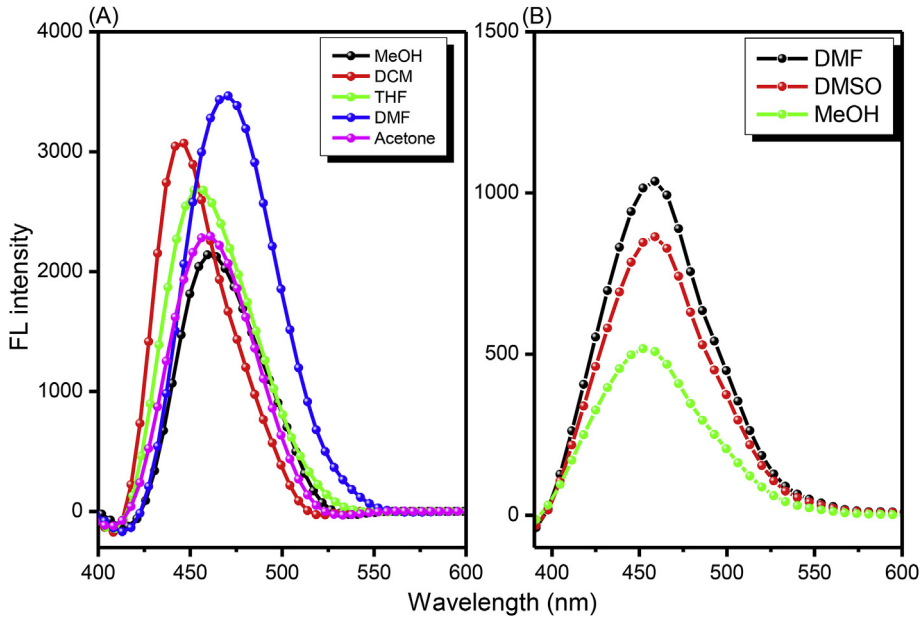

Fig. 5. PL spectra of (A) pyrene-2NH_2 and (B) pyrene-PTyr under the excitation wavelength (343 nm).

state was measured to be 40.

3.4. Aggregation-induced emission

We examined the AIE effects of pyrene-2NH_2 and the polypeptide pyrene-PTyr by varying their concentrations and using various solvent/nonsolvent pairs. To evaluate the effect of concentration on the fluorescence emission of pyrene-2NH_2 and the polypeptide pyrene-PTyr, we measured their fluorescence at various concentrations in DMF and methanol. Fig. 6A and B reveal that the emission intensities decreased upon increasing the concentration of pyrene-2NH_2 in DMF and methanol, respectively. This "concentration-quenched emission" of pyrene-2NH_2 is mainly arose from the strong face-to-face π–π interactions of pairs of pyrene units, leading to the formation of dimers that functioned as excimers, which were readily quenched. On the other hand, Fig. 6C and D reveal that the fluorescence emission of the polypeptide pyrene-PTyr was very weak in dilute solution (10^{-5} M) in DMF and methanol, but increasing the concentration of pyrene-PTyr from 10^{-4} to 10^{-2} M was accompanied by increasing fluorescence emissions in both solvents. This "concentration-enhanced emission" was presumably caused by the AIE effect. In light of these results, the fluorescence behavior of pyrene-2NH_2 may transform from ACQ to AIE after its conjunction into the PTyr main chain. The ACQ effect of pyrene-2NH_2 and the AIE effect of pyrene-PTyr were confirmed by measuring their fluorescence emissions in solvent/nonsolvent pairs. We studied the fluorescence behavior of pyrene-2NH_2 in the solvent/nonsolvent

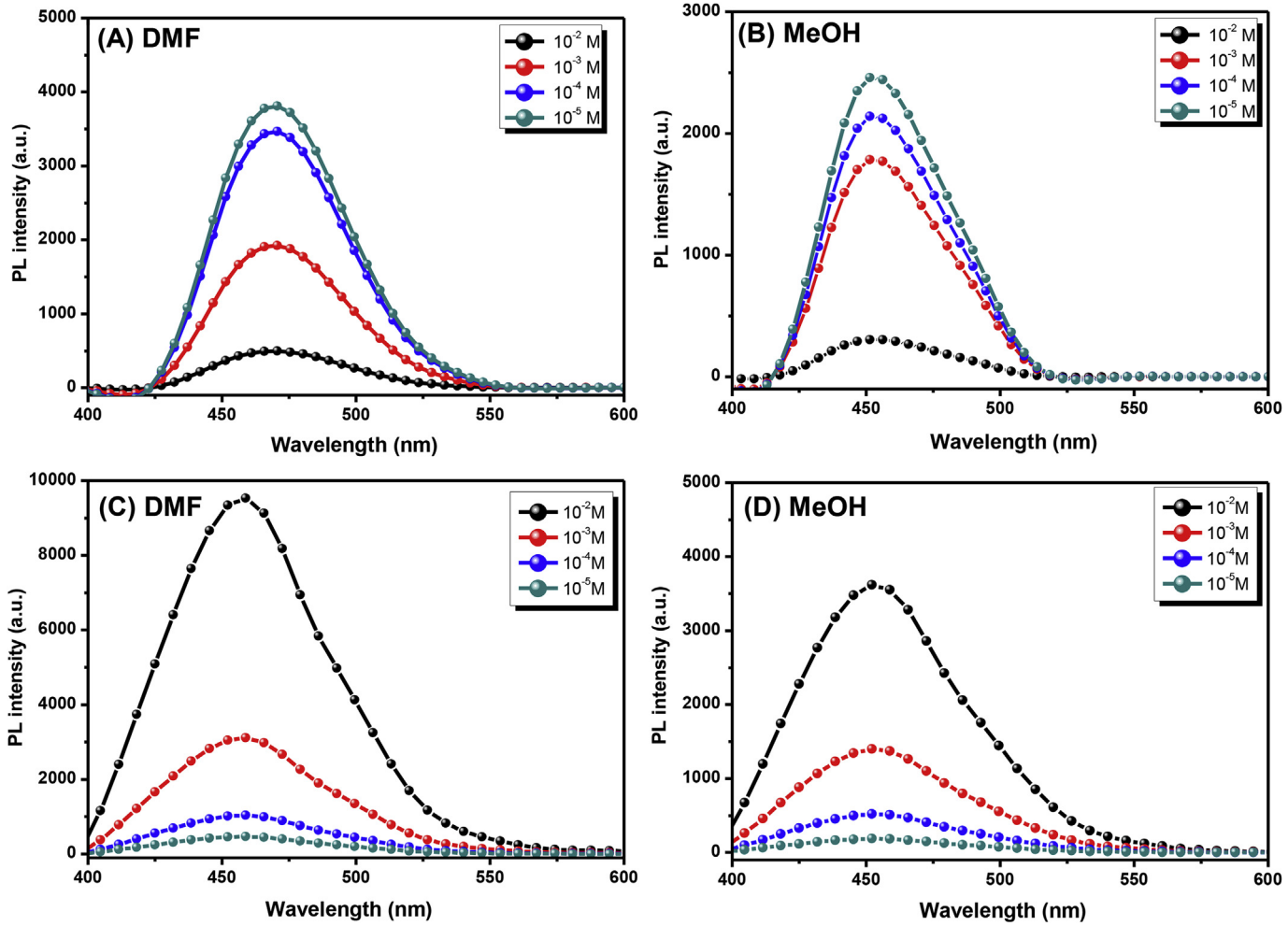

Fig. 6. PL spectra of (A) pyrene-2NH_2 in DMF, (B) pyrene-2NH_2 in methanol, (C) pyrene-PTyr in DMF, and (D) pyrene-PTyr in methanol at different concentrations (excitation wavelength: 343 nm).

pair of DMF/water (Fig. 7A and C). Pyrene-2NH_2 exhibited a strong emission as a dilute solution (10^{-4} M) in DMF, but increasing the concentration of water resulted in a decrease in its fluorescence emission. We studied the fluorescence behavior of the polypeptide pyrene-PTyr in methanol/toluene pairs (Fig. 7B and D). Here, we avoided DMF as a solvent for the polypeptide pyrene-PTyr to obviate any hydrogen bonding interaction between polypeptide and DMF. Interestingly, the fluorescence intensities of pyrene-PTyr increased upon increasing the toluene concentrations over the range from 20 to 80 vol%, due to aggregation, consistent with AIE behavior. Additionally, to further confirm the AIE behavior of pyrene-PTyr, we investigated the fluorescence of pyrene-PTyr polypeptide in the solid state. As shown in Fig. S4, pyrene-PTyr exhibited a massive fluorescence emission peak at 458 nm which strongly confirmed the AIE behavior of pyrene-PTyr polypeptide. Thus, these experiments confirmed that the polypeptide pyrene-PTyr exhibits AIE behavior, whereas pyrene-2NH_2 displays ACQ behavior.

Generally, the AIE phenomenon could mechanistically be associated with various pathways as J-aggregate formation (JAF) [59], restriction of intramolecular rotation (RIR) [60], excited-state intramolecular proton transfer (ESIPT) [61], the restriction of charge transfer (CT), and twisted intramolecular charge transfer (TICT) [62]. Pyrene containing polymers with AIE behavior have been previously reported and their AIE mechanism ascribe to the RIR, in which the formation of aggregates forced the physical restraints on the intramolecular rotations [63]. As previously reported, the formed aggregates enhanced the radiative excitons and prevent the non-radiative channels, thereby the fluorescence emission strongly increased in the aggregated (solid) state [64]. Therefore, the mechanism of the transition from aggregation-caused quenching (ACQ) behavior of pyrene-2NH2 to aggregation-induced emission (AIE) after incorporation into the rigid rod chains of polytyrosine can be accounted for the RIR mechanism. Pyrene-2NH_2 possessing a flexible C-C bond between the pyridyl and amino groups, which can dynamic intramolecular rotate (IR), leading to strongly quench of its excited states and then absence of its luminescence. After the incorporation of Pyrene-2NH_2 into the pyrene-PTyr, the polypeptide side chain and C-C bond of our pyrene-PTyr can freely rotate in the dilute solution, while in the concentrated solution or aggregate (solid) state that rotation would be restrained completely and then enhanced the fluorescence emission (Scheme 1). Therefore, the AIE behavior of our polypeptide pyrene-PTyr can be accounted for the RIR mechanism.

3.5. Thermal behavior of pyrene-PTyr/P4VP blends

Miscible blends of biomaterial polymers and non-biomaterial polymers have a wide range of biomedical applications [65,66]. We used DSC to study the blending ability of the polypeptide pyrene-PTyr with P4VP. Fig. 8A displays DSC thermal analyses of pyrene-PTyr/P4VP blends. The pure pyrene-PTyr polypeptide exhibited a glass transition temperature (T_g) of 157 °C, similar to that of linear PTyr [24], due to the planar structure of the pyrene-2NH_2 initiator. All of the pyrene-PTyr/P4VP blends in this study displayed the single T_g, indicating complete miscibility for these blend systems. Fig. 8A also reveals that

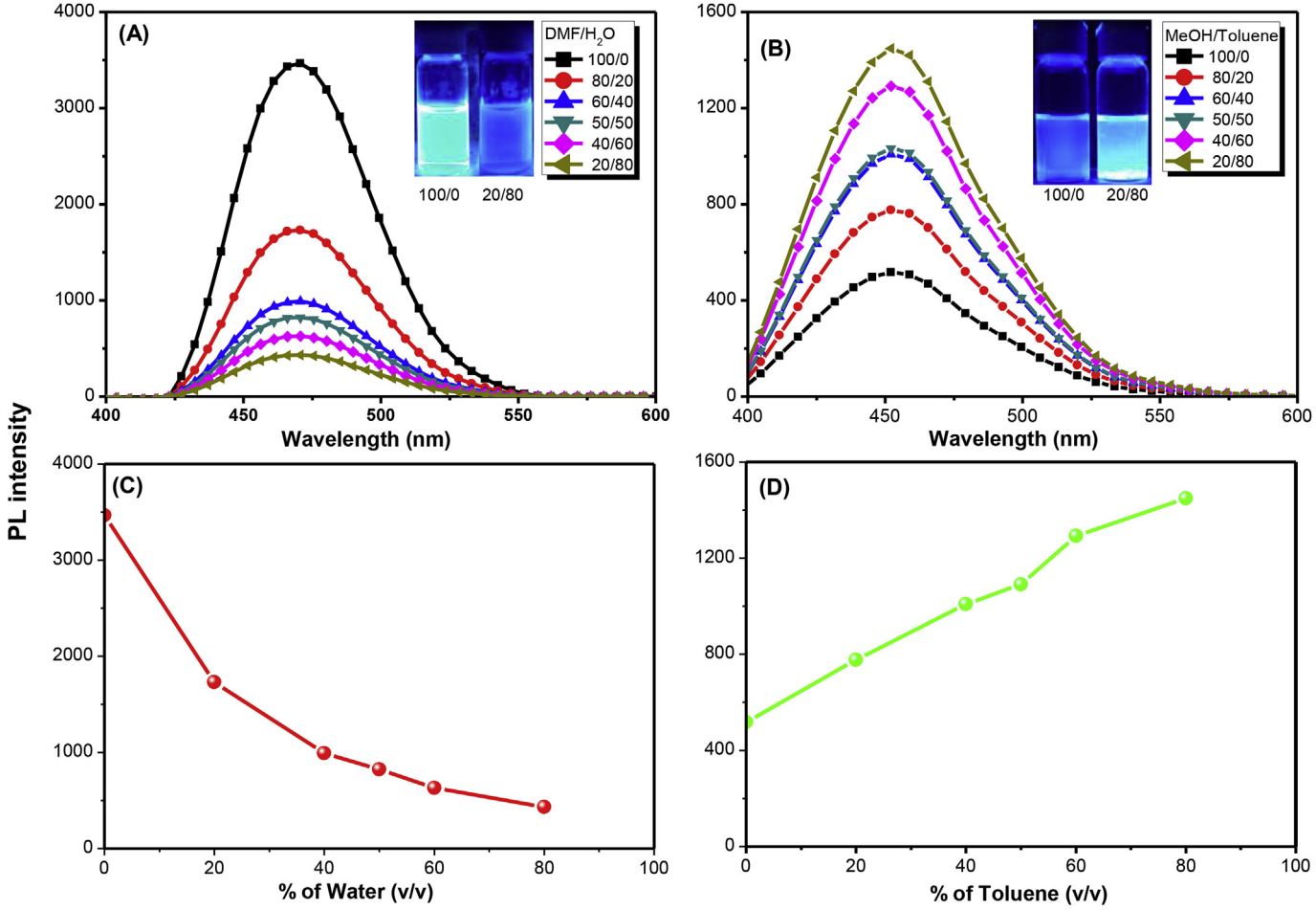

Fig. 7. The solution PL emission spectra of (A) pyrene-2NH_2 in DMF-H_2O and (B) pyrene-PTyr in methanol-toluene, and the PL emission intensities of (C) pyrene-2NH_2 in DMF-H_2O and (D) pyrene-PTyr in methanol-toluene versus nonsolvent fraction.

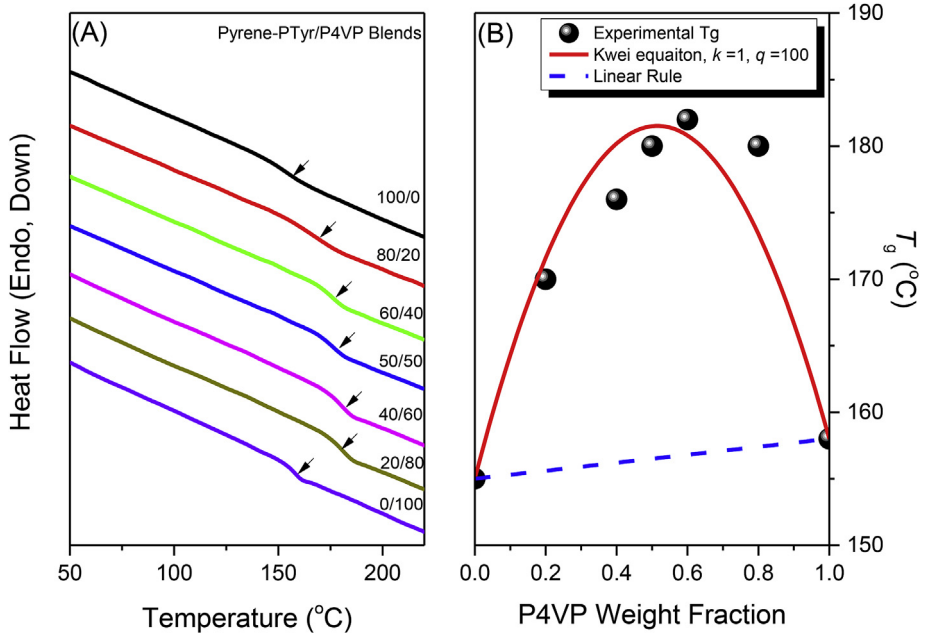

Fig. 8. (A) DSC thermograms of pyrene-PTyr/P4VP blends and (B) the T_g plot of pyrene-PTyr with the content increasing of P4VP.

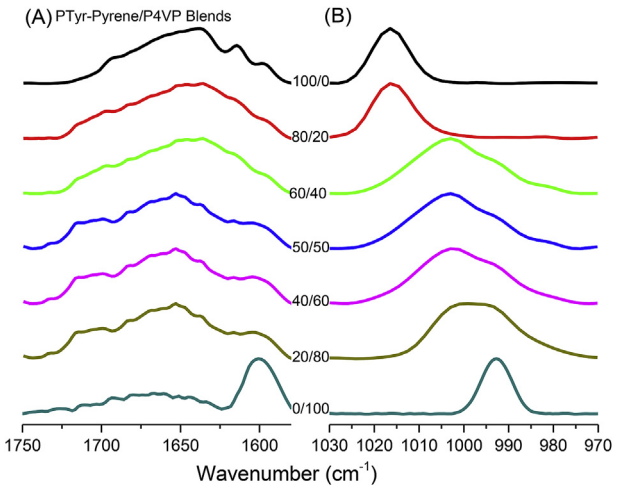

Fig. 9. (A) FTIR spectra of the pyrene-PTyr/P4VP blends: (A) 1750–1550 cm^{-1} and (B) 1030–970 cm^{-1} measured at room temperature.

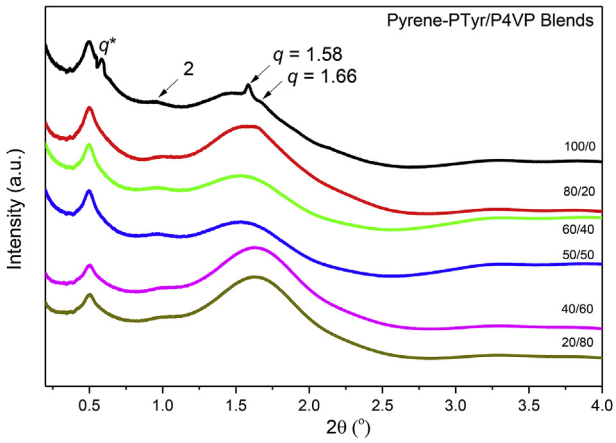

Fig. 11. WAXD patterns of pyrene-PTyr blends with P4VP.

the T_g values of pyrene-PTyr/P4VP miscible blends were increased upon increasing the content of P4VP, consistent with strong hydrogen bonding in pyrene-PTyr/P4VP blends. Fig. 8B presents a T_g–composition plot of these miscible pyrene-PTyr/P4VP blends; it reveals that the T_g values were positively greater than those predicted from the means of linear rule. Moreover, the T_g–composition relationships of the pyrene-PTyr/P4VP miscible blends followed the Kwei equation [67]:

$$T_g = \frac{W_1 T_{g1} + kW_2 T_{g2}}{W_1 + kW_2} + qW_1 W_2$$

where k or q is fitting constant; W_1 or W_2 is the weight fraction of pyrene-PTyr and P4VP, respectively; and T_{g1} or T_{g2} is the glass transition temperature of pyrene-PTyr and P4VP, respectively. We obtained values of k and q of 1 and 100 from the non-linear fitting approach. The positive value of q confirmed that a strong interaction existed between pyrene-PTyr and P4VP, much more potent than the self-association of the phenolic OH units in the polypeptide pyrene-PTyr.

3.6. Hydrogen bonding and secondary structures of pyrene-PTyr/P4VP blends

FTIR spectroscopy is a simple, facile, and rapid technique for studying noncovalent interactions in the secondary structures of polypeptides and specific polymers [68,69]. Here, we used FTIR spectroscopy to investigate the hydrogen bonding interactions and also used to investigate the secondary structures of pyrene-PTyr/P4VP blends in solid state. Fig. 9A and B displays room-temperature FITR analyses of pyrene-PTyr/P4VP miscible blends with various weight ratios, in the regions 1750–1550 cm^{-1} (amide absorption) and 1030–970 cm^{-1} (pyridine absorption), respectively. The spectrum of pure pyrene-PTyr featured a clear band at 1016 cm^{-1}, while pure P4VP provided an absorption band at 993 cm^{-1}. We monitored the hydrogen bonding between pyrene-PTyr and P4VP by observing the shift in the wavenumber of the absorbance band of pyridyl ring (initially at 993 cm^{-1}). The P4VP signal at 993 cm^{-1} shifted to higher wavenumber

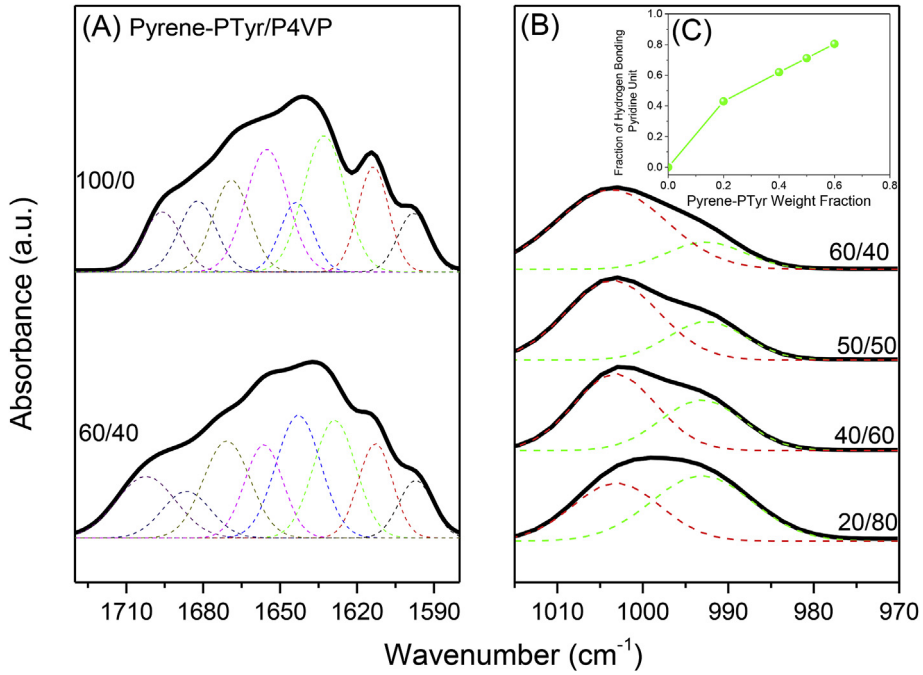

Fig. 10. Curve fitting results of FTIR spectra for Pyrene-PTyr/P4VP blends: (A) amide I unit region, (B) pyridine unit region, and (C) the fraction of hydrogen bonding of pyridine unit within P4VP.

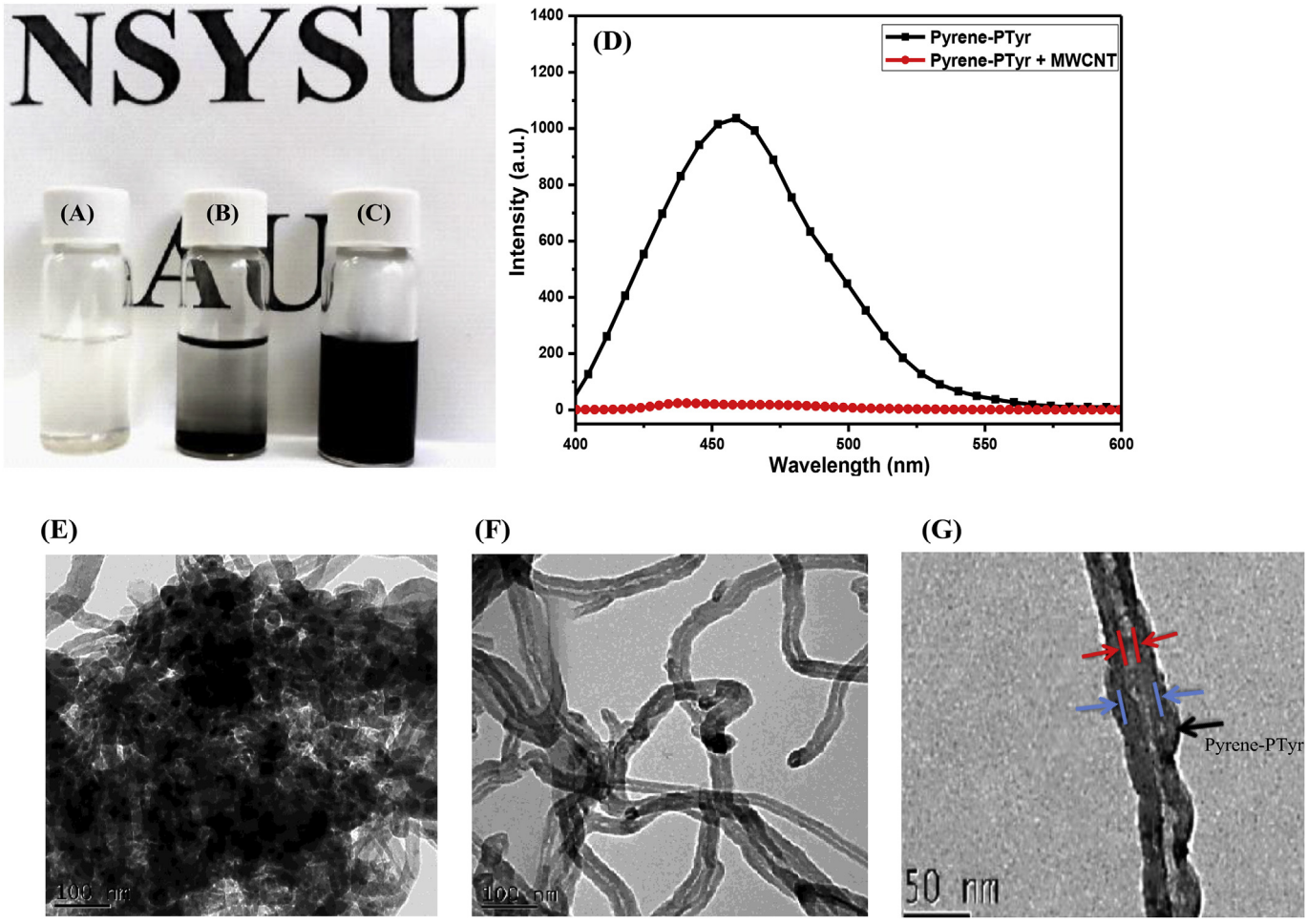

Fig. 12. Photographs of (A) pyrene-PTyr, (B) MWCNT, (C) pyrene-PTyr/MWCNT dispersions in DMF. (D) PL emission spectra of pyrene-PTyr and pyrene-PTyr/MWCNT in DMF (excitation wavelength: 343 nm). TEM photo-images of (E) Pristine MWCNT after sonication in DMF and the pyrene-PTyr/MWCNT dispersion on (F) large and (G) small scales.

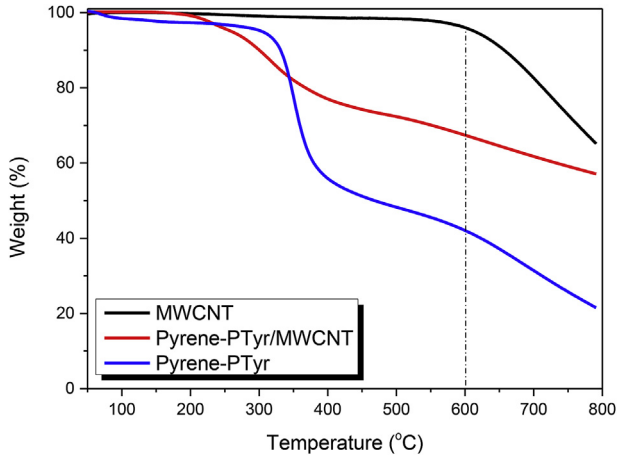

Fig. 13. TGA analyses of pyrene-PTyr, MWCNT and pyrene-PTyr/MWCNT.

(1003 cm^{-1}) after blending with pyrene-PTyr, suggesting strong hydrogen bonding in pyrene-PTyr/P4VP blends. We also used these two peaks to digitally construe the hydrogen bonding interactions through digital subtraction of the peak at 1016 cm^{-1} for pure pyrene-PTyr, based on weight fractions of the polypeptide pyrene-PTyr in the blend systems. Fig. 10(B) presents the outcomes of curve fitting results; the hydrogen-bonded pyridyl fraction was increased upon increasing the compositions of pyrene-PTyr in blends (Fig. 10(C)).

To identify the change in secondary structure, we monitored the eight major peaks of the pure pyrene-PTyr: 1598 and 1613 cm^{-1} for the Tyr ring vibration; 1655 cm^{-1} for the α-helical; 1631 cm^{-1} for β-sheet; 1669 cm^{-1} for β-turn; and 1643, 1682, and 1696 cm^{-1} for the random coil conformations. When we blended our polypeptide with 40 wt% of P4VP, where the contents of the α-helical and β-sheet secondary structures was decreased, while the contents of the random coil conformation was increased from 26.8 to 38.3% (Fig. 10A). We also investigated the secondary structures of the pyrene-PTyr/P4VP blends by measuring their X-rays patterns. The pure pyrene-PTyr having a degree of polymerization of 14 was present as a β-sheet secondary structure, based on the Bragg diffraction pattern (Fig. 11). We also observed a q value of 0.57, attributed to the intertublar distance (d = 1.09 nm) among the pyrene-PTyr backbones within antiparallel β-sheet structures. Moreover, the diffraction peak at a q value of 1.58 corresponded to the intermolecular distance (d = 0.394 nm) between adjacent polypeptide pyrene-PTyr chains within the one lamellar structure; the peak at a q value of 1.66 corresponded to repeated residue of pyrene-PTyr chain (d = 0.375 nm). Upon further increasing the P4VP content in pyrene-PTyr blends, the WAXD pattern of pyrene-PTyr transformed into a broad amorphous halo and the signals due to β-sheet conformation disappeared.

3.7. Fabrication of MWCNT composites and CNT dispersions

CNTs can be difficult to disperse due to the strong π-stacking of their tubes, leading to high degrees of aggregation. One of the most useful methods for improving the dispersion of CNTs is the use of polymers or polypeptides containing specific moieties capable of strong π-stacking (e.g., pyrene), such that they interact noncovalently with the CNTs. Accordingly, we investigated the applicability of our polypeptide pyrene-PTyr for the dispersion of CNTs. Fig. 12(A)–(C) display photographs of DMF solutions of the pure pyrene-PTyr, the pristine MWCNTs, and the pyrene-PTyr/MWCNT complex, after sonication for 1 h and the standing for 24 h. The pure pyrene-PTyr formed a transparent solution, whereas the pristine MWCNTs precipitated completely. In contrast, the solution of the pyrene-PTyr/MWCNT complex did not feature any precipitate, suggesting the presence of strong interactions between the pyrene moieties of the polypeptide and the MWCNTs through π-stacking. This behavior was confirmed in Fig. 12(D), which displays the fluorescence spectra of the polypeptide pyrene-PTyr and the pyrene-PTyr/MWCNT complex in DMF after excitation at 343 nm. The spectrum of the pure pyrene-PTyr exhibited a strong fluorescence signal at 385 nm, due to the presence of its pyrene moieties, while that of the pyrene-PTyr/MWCNT complex featured a very weak fluorescence emission, confirming the presence of interactions between pyrene groups with MWCNTs. We attribute the quenched fluorescence of the pyrene-PTyr/MWCNT complex to energy transfer from the light-emitted pyrene moieties to the MWCNTs [70]. Moreover, TEM confirmed the presence of interactions between the polypeptide and the MWCNTs [Fig. 12(E)–(G)]. The TEM image of the pristine MWCNTs in DMF revealed a high degree of aggregation, due to self π–π interactions, whereas that of the pyrene-PTyr/MWCNT dispersion revealed a uniform dispersion of MWCNTs, presumably stabilized through intermolecular noncovalent interactions. Thus, we our new polypeptide pyrene-PTyr was indeed efficient at dispersing MWCNTs and should, therefore, be of further use as a dispersing agent for various applications. We examined the thermal stabilities of the polypeptide pyrene-PTyr and the pyrene-PTyr/MWCNT complex through TGA, from 80 to 800 °C under the N_2. Fig. 13 reveals that the pure polypeptide pyrene-PTyr provided a char yield of 21%, while the pyrene-PTyr/MWCNT complex exhibited a char yield of 58% (approximately the same as that of the pristine MWCNTs). The content of pyrene-PTyr in the pyrene-PTyr/MWCNT complex was calculated, based on the char yields of the MWCNTs and pyrene-PTyr, to be 28%.

4. Conclusion

We have used 1,6-diaminopyrene (pyrene-2NH_2) as an initiator for the facile synthesis of the polypeptide pyrene-PTyr through the ROP of Tyr-NCA. PL spectra revealed that pyrene-2NH_2 is the ACQ material, while it was transformed into the strong AIE material after incorporation into the rod rigid backbone of the polypeptide pyrene-PTyr. Blending pyrene-PTyr with various weight ratios of P4VP resulted in completely miscible blends displaying single glass transition temperatures, based on DSC analyses. In FTIR spectra, shifting of the pyridine signal of P4VP after blending with pyrene-PTyr confirmed the strong hydrogen bonding in pyrene-PTyr/P4VP blends. Furthermore, FTIR spectral and WAXD data revealed that the polypeptide pyrene-PTyr converted from β-sheet conformation to the random coil when blending with P4VP homopolymer. Moreover, we prepared pyrene-PTyr/MWCNT complexes stabilized through π–π interaction between the pyrene groups of pyrene-PTyr and surfaces of MWCNTs. PL spectroscopy revealed that the fluorescence quenching of the pyrene-PTyr/MWCNT complexes was due to energy transfer from the pyrene moieties to the MWCNTs. TEM imaging confirmed that pyrene-PTyr is an efficient dispersant for MWCNTs. This new polypeptide pyrene-PTyr, displaying AIE behavior and capable of strong π-stacking, should be of interest when applied to biomedical applications.

Acknowledgment

This study was supported financially by the Ministry of Science and Technology, Taiwan, under contracts MOST 106-2221-E-110-067-MY3 and 105-2221-E-110-092-MY3.

Appendix A. Supplementary data

Supplementary data to this article can be found online at https://doi.org/10.1016/j.polymer.2018.09.052.

References

[1] B. Tian, X.G. Tao, T.Y. Ren, Y. Weng, X. Lin, Y. Zhang, X. Tang, J. Mater. Chem. 22 (2012) 17404–17414.
[2] Y. Hirano, D.J. Mooney, Adv. Mater. 16 (2004) 17–25.
[3] E. Jeevithan, Z. Jingyi, B. Bao, W. Shujun, R. JeyaShakila, W.H. Wu, RSC Adv. 6 (2016) 14236–14246.
[4] H.R. Kricheldorf, Angew. Chem. Int. Ed. 45 (2006) 5752–5784.
[5] T.J. Deming, Prog. Polym. Sci. 32 (2007) 858–875.
[6] P. Papadopoulous, G. Floudas, A.H. Klok, I. Schnell, T. Pakula, Biomacromolecules 5 (2004) 81–91.
[7] C. He, X. Zhuang, Z. Tang, H. Tian, X. Chen, Adv. Healthc. Mater. 1 (2012) 48–78.
[8] N. Hadjichristidis, H. Iatrou, M. Pitsikalis, G. Sakellariou, Chem. Rev. 109 (2009) 5528–5578.
[9] P.C. Li, Y.C. Lin, M. Chen, S.W. Kuo, Soft Matter 9 (2013) 11257–11269.
[10] X. Fu, Y. Shen, W. Fu, Z. Li, Macromolecules 46 (2013) 3753–3760.
[11] S.W. Kuo, H.F. Lee, C.F. Huang, C.J. Huang, F.C. Chang, J. Polym. Sci., Part A: Polym. Chem. 46 (2008) 3108–3119.
[12] C. Hua, C.M. Dong, Y. Wei, Biomacromolecules 10 (2009) 1140–1148.
[13] Y.C. Lin, S.W. Kuo, Polym. Chem. 3 (2012) 162–171.
[14] S.W. Kuo, H.F. Lee, W.J. Huang, K.U. Jeong, F.C. Chang, Macromolecules 42 (2009) 1619–1626.
[15] S.W. Kuo, J. Polym. Res. 15 (2008) 459–486.
[16] Y. Xu, W. Yu, C. Zhou, RSC Adv. 4 (2014) 55435–55444.
[17] S.W. Kuo, W.J. Huang, C.F. Huang, S.C. Chan, F.C. Chang, Macromolecules 37 (2004) 4164–4173.
[18] C.T. Pan, C.K. Yen, H.C. Wu, L.W. Lin, Y.S. Lu, J.C.C. Huang, S.W. Kuo, J. Mater. Chem. 3 (2015) 6835–6843.
[19] S.W. Kuo, C.F. Huang, P.H. Tung, W.J. Hunag, J.M. Hunag, F.C. Chang, Polymer 46 (2005) 9348–9361.
[20] J.V. Barth, J. Weckesser, C.Z. Cai, P. Gunter, L. Burgi, O. Jeandupeux, K. Kern, Angew. Chem. Int. Ed. 39 (2000) 1230–1234.
[21] S. Yoshimoto, N. Yokoo, T. Fukuda, N. Kobayashi, K. Itaya, Chem. Commun. 5 (2006) 500–502.
[22] S.W. Kuo, C.J. Chen, Macromolecules 44 (2011) 7315–7326.
[23] S.W. Kuo, C.J. Chen, Macromolecules 45 (2012) 2442–2452.
[24] Y.S. Lu, Y.C. Lin, S.W. Kuo, Macromolecules 45 (2012) 6547–6556.
[25] B. Valeur, Molecular Fluorescence: Principles and Applications, Wiley, Weinheim, Germany, 2002.
[26] B. Valeur, M.N. Berberan-Santos, J. Chem. Educ. 88 (2011) 731–738.
[27] M. Xavier, P. Fabien, L.D. Thilo, D. Maxime, B.P. Marcel, A.A. Paul, W. Shimon, Single Mol. 2 (2001) 261–276.
[28] S.Y. Park, J.H. Yoon, C.S. Hong, R. Souane, J.S. Kim, S.E. Mattews, J. Vicens, J. Org. Chem. 73 (2008) 8212–8218.
[29] Y. Zhou, C.Y. Zhu, X.S. Gao, X.Y. You, C. Yao, Org. Lett. 12 (2010) 2566–2569.
[30] P. Conlon, C.J. Yang, Y. Wu, Y. Chan, K. Martinez, Y. Kim, N. Stevens, A.A. Marti, S. Jockusch, N.J. Turro, W. Tan, J. Am. Chem. Soc. 130 (2008) 336–342.
[31] J.T. Hutt, Z.D. Aron, J. Chem. Educ. 91 (2014) 1990–1994.
[32] R.A. Blatchly, Z. Delen, P.B. O'Hara, J. Chem. Educ. 91 (2014) 1623–1630.
[33] P. Marks, M. Levine, J. Chem. Educ. 89 (2012) 1186–1189.
[34] S.A. Jenekhe, J.A. Osaheni, Science 265 (1994) 765–768.
[35] H.F. Xiang, J.H. Cheng, X.F. Ma, X.G. Zhou, J.J. Chruma, Chem. Soc. Rev. 42 (2013) 6128–6185.
[36] J. Luo, Z. Xie, J.W.Y. Lam, L. Cheng, H. Chen, C. Qiu, H.S. Kwok, X. Zhan, Y. Liu, D. Zhu, B.Z. Tang, Chem. Commun. 18 (2001) 1740–1741.
[37] Z. Zhao, S. Chen, J.W.Y. Lam, P. Lu, Y. Zhong, K.S. Wong, H.S. Kwok, B.Z. Tang, Chem. Commun. 46 (2010) 2221–2223.
[38] J. Liu, Y. Zhong, J.W. Lam, Y. Lam, P. Lu, Y. Hong, Y. Yu, Y. Yue, M. Faisal, H.H.Y. Sung, I.D. Williams, Macromolecules 43 (2010) 4921–4936.
[39] S.T. Li, Y.C. Lin, S.W. Kuo, W.T. Chuang, J.L. Hong, Polym. Chem. 3 (2012) 2393–2402.
[40] M.F.L. De Volder, S.H. Tawfick, R.H. Baughman, J. Hart, Science 339 (2013) 535–539.
[41] C. Ehli, G.M.A. Rahman, N. Jux, D. Balbinot, D.M. Guldi, F. Paolucci, M. Marcaccio, D. Paolucci, M. Melle-Franco, F. Zerbetto, S.P. Campidelli, M. Prato, J. Am. Chem. Soc. 128 (2006) 11222–11231.
[42] K.C. Etika, F.D. Jochum, P. Theato, J.C. Grunlan, J. Am. Chem. Soc. 131 (2009) 13598–13599.
[43] Y.K. Baek, D.H. Jung, S.M. Yoo, S. Shin, J.H. Kim, H.J. Jeon, Y.K. Choi, S.Y. Lee, H.T. Jung, J. Nanosci. Nanotechnol. 11 (2011) 4210–4216.
[44] A.M. Münzer, W. Seo, G.J. Morgan, Z.P. Michael, Y. Zhao, K. Melzer, G. Scarpa, J.

Phys. Chem. C 118 (2014) 17193–17199.
[45] L. Henrard, E. Hernandez, P. Bernier, A. Rubio, Phys. Rev. B Condens. Matter 60 (1999) R8521–R8524.
[46] S. Wang, E.S. Humphreys, S.Y. Chung, D.F. Delduco, S.R. Lustig, H. Wang, K.N. Parker, N.W. Pizzo, S. Subramoney, Y.M. Chiang, A. Jagota, Nat. Mater. 2 (2003) 196–200.
[47] Y. Yao, W. Li, S. Wang, D. Yan, X. Chen, Macromol. Rapid Commun. 27 (2006) 2019–2025.
[48] J. Chen, M.A. Hamon, H. Hu, Y.S. Chen, A.M. Rao, P.C. Eklund, R.C. Haddon, Science 282 (1998) 95–98.
[49] V. Zorbas, A. Ortiz-Acevedo, A.B. Dalton, M.M. Yoshida, G.R. Dieckmann, R.K. Draper, R.H. Baughman, M. Jose-Yacaman, I.H. Musselman, J. Am. Chem. Soc. 126 (2004) 7222–7227.
[50] S. Wang, E.S. Humphreys, S.Y. Chung, D.F. Delduco, S.R. Lustig, H. Wang, K.N. Parker, N.W. Rizzo, S. Subramoney, Y.M. Chiang, A. Jagota, Nat. Mater. 2 (2003) 196–200.
[51] S.R. Whaley, D.S. English, E.L. Hu, P.F. Barbara, A.M. Belcher, Nature 405 (2000) 665–668.
[52] Y.R. Jheng, M.G. Mohamed, S.W. Kuo, Polymers 9 (2017) 503.
[53] M.G. Mohamed, F.H. Lu, J.L. Hong, S.W. Kuo, Polym. Chem. 6 (2015) 6340–6350.
[54] C.Y. Tsai, C.H. Chung, J.L. Hong, ACS Omega 3 (2018) 4423–4432.
[55] K. Kalyanasundaram, J.K. Thomas, J. Am. Chem. Soc. 99 (1977) 2039–2044.
[56] E.M.S. Castanheira, J.M.G. Martinho, Chem. Phys. Lett. 185 (1991) 319–323.
[57] F.M. Winnik, Chem. Rev. 93 (1993) 587–614.
[58] A. Ghosh, A. Sengupta, A. Chattopadhyay, D. Das, Chem. Commun. 51 (2015) 11455–11458.
[59] B. Birks, Photophysics of Aromatic Molecules, Wiley, London, 1970.
[60] Y.N. Hong, J.W.Y. Lam, B.Z. Tang, Chem. Commun. 58 (2009) 4332.
[61] V.S. Padalkar, S. Seki, Chem. Soc. Rev. 45 (2016) 169–202.
[62] Y. Hong, J.W.Y. Lam, B.Z. Tang, Chem. Soc. Rev. 40 (2011) 5361–5388.
[63] Y. Dong, Z. Yang, Z. Ren, S. Yan, Polym. Chem. 6 (2015) 7827–7832.
[64] Y. Ren, J.W.Y. Lam, Y.Q. Dong, B.Z. Tang, K.S. Wong, J. Phys. Chem. B 109 (2005) 1135–1140.
[65] S.C. Neves, L.S. Moreira Teixeira, L. Moroni, R.L. Reis, C.A. van Blitterswijk, N.M. Alves, M. Karperien, J.F. Mano, Biomaterials 32 (2011) 1068–1079.
[66] H. Bodugoz-Senturk, C.E. Macias, J.H. Kung, O.K. Muratoglu, Biomaterials 30 (2009) 589–596.
[67] T.K. Kwei, J. Polym. Sci., Polym. Lett. Ed. 22 (1984) 307–313.
[68] X.G. Chen, R. Schweitzer-Stenner, S.A. Asher, N.G. Mirkin, S. Krimm, J. Phys. Chem. B 99 (1995) 3074–3083.
[69] R. Schweitzer-Stenner, G. Sieler, N.G. Mirkin, S. Krimm, J. Phys. Chem. 102 (1998) 118–127.
[70] K.W. Huang, Y.R. Wu, K.U. Jeong, S.W. Kuo, Macromol. Rapid Commun. 34 (2013) 1530–1536.